Fully Inkjet-Printed VO2\n-Based Radio-Frequency Switches for Flexible Reconfigurable Components

DOI: 10.1002/ ((please add manuscript number))
Article type: Full Paper

Fully Inkjet-Printed VO_2-Based Radio-Frequency Switches for Flexible Reconfigurable Components

Shuai Yang, Mohammad Vaseem, and Atif Shamim*

Mr. S. Yang, Dr. M. Vaseem, Prof. A. Shamim
King Abdullah University of Science and Technology (KAUST), IMPACT Lab, Computer, Electrical and Mathematical Sciences and Engineering (CEMSE) Division, Thuwal 23955-6900, Kingdom of Saudi Arabia
E-mail: shuai.yang@kaust.edu.sa

Keywords: VO_2, RF switches, inkjet printing, MIT, additive manufacturing

Frequency-reconfigurable radio-frequency (RF) components are in high demand due to multiple frequency-bands in wireless devices as well as varying frequency-spectrum standards across the world. An important part of reconfigurable components is a switch; however, existing switches are very expensive, particularly for higher frequencies (~10s of dollars). In this regard, metal-insulator transition (MIT) materials are attractive, as they can change their phase and can be used as switches. Vanadium dioxide (VO_2) is one of such material that features a transition temperature of only 68 °C. The cost of the switch can be brought down considerably (~cents), if MIT materials such as VO_2 can be inkjet-printed; however, no ink of this sort is commercially available. In this work, we present, for the first time, VO_2 ink and fully printed RF switches (shunt and series configurations) through this ink. Both thermal and electrical triggering mechanisms have been investigated in this work. These switches have shown decent performance up to 40 GHz. A more than 10^2 ON/OFF ratio and a switching speed of 0.4 µs have been achieved. Finally, a frequency-reconfigurable antenna, printed on a flexible Kapton substrate along with a printed VO_2 switch, has been demonstrated as a proof of concept.

1. Introduction

The wireless industry is seeing demand for tunable and re-configurable radio-frequency (RF) components (such as antenna and filters), which can be tuned to different frequency bands on demand. There are two primary reasons for this drive: (1) RF components such as antennas and filters are typically large in size and occupy a large area in any wireless device. In present wireless devices such as mobile phones, many of these filters and antennas are required for different bands, such as global system for mobile communications (GSM) (900 MHz, 1800 MHz), 3G/4G (2 to 3 GHz, typically), global positioning system (GPS) (1.5 GHz), WiFi (2.4 and 5 GHz) and so on. If instead of these bands being covered by five or six antennas, one or two could be reconfigured to cover them, substantial space and cost savings could be achieved. (2) The wireless standards (frequency bands of operation) vary slightly in different parts of the world. In order to have a global device that can be adjusted to varying wireless standards in different parts of the world, the RF components need to be tuned to these frequency bands. Clearly, tunable or reconfigurable RF components are in demand. This tuning is typically done through an RF switch, which is capable of blocking or allowing RF signals to pass through it based on applied stimuli.

Several kinds of technologies are used for RF-switching applications, such as a PIN diode-based switch,[1,2] a microelectromechanical-systems-based (MEMS-based) switch,[3,4] a transistor-based switch,[5,6] ferrite- and ferro-electric based devices[7,8] and so on. Each has its advantages and disadvantages; for instance, PIN diode switches feature fast switching speeds and longer operation life, but they can handle only relatively low power, and also they cannot work at very low frequencies. By contrast, while MEMS based switches are very attractive for applications where isolation and insertion loss are the essential requirements, their slow switching speeds and relatively short operating life makes them unsuitable for applications that

need fast and frequent switching. The most important drawback of the available switches, however, is that most of them have been realized through expensive fabrication methods that require complicated and time-consuming processing steps, as well as expensive materials and tools, and thus the cost of an individual switch is high. The cost of the switch is further increased as the frequency of operation increases. For example, RF switch (SKY13408-465LF) from Skyworks Solutions Inc. has an operating frequency of 1–6 GHz, which features 24 dB isolation and 1.1 dB insertion loss at 6 GHz. The unit price listed on Digikey is USD 2.45.[9] Another commercially available RF switch, based on metal–semiconductor field-effect transistor (MESFET) nanofabrication technology, is HMC1084LC4 from Analog Devices Inc. It operates from 23 GHz to 30 GHz, with an isolation of 26 dB and an insertion loss of 3.3 dB, but it costs around USD 38.[10]

Recently, phase-change materials such as vanadium dioxide (VO_2) or chalcogenides have been recognized as interesting alternatives for switching applications, as their electrical properties can be tuned with heat or current.[11,12] Vanadium dioxide has drawn more attention because it exhibits metal-insulator transition (MIT) in a reversible fashion, and that too at a relatively lower temperature of 68 °C.[13] This makes VO_2 a promising material for high-speed switching and reconfigurable devices. A few studies have demonstrated RF switches using VO_2 material. For example, H. Madan et al. fabricated a VO_2 RF switch that can work up to 50 GHz with an isolation of 35 dB and insertion loss of 0.5 dB. However, their VO_2 film is deposited by a metalorganic molecular beam epitaxy (MOMBE) deposition technique.[14] Sieu D. Ha et al. reported a VO_2 switch that has 25 dB of isolation and 3 dB of insertion loss, up to 13.5 GHz; however, this has also been fabricated with expensive nanofabrication methods, precisely through RF sputtering.[15] Other reports also showed VO_2 switches perform at high frequencies, but the VO_2 is either deposited using pulsed laser deposition (PLD) or e-beam evaporation.[16–18] The VO_2 deposition techniques such as MOMBE, sputter, PLD or evaporation, all require a

high level of vacuum conditions, and sometimes very high processing temperatures. Also, these processes require expensive masks. Overall, the existing VO_2 switches in the literature have the same issue as that of the commercial switches, namely high cost.

In contrast to the above-mentioned subtractive technologies, additive manufacturing techniques (inkjet, screen and 3D printing) offer extremely low cost, completely digital and highly scalable manufacturing processes.[19] Due to these advantages, additive manufacturing techniques have been used to realize sensors,[20–24] transistors,[25–29] RF inductors,[30–33] RF capacitors,[30,32,34–36] RF filters,[32,37–39] RF identification (RFID) tags[40–44] and so on. There have only been a few reports on printed RF switches.[45–47] A MEMS-based switch as has been reported;[47] however, the fabrication process involves non-printing step (acid etching step to be precise); thus, the paper does not qualify for fully printed RF switch work. Moreover, complete RF characterization of the switch and its capability to turn ON and OFF multiple times for practical switching operation has not been shown. The other works on printed RF switches are based on printed carbon nanotube field-effect transistor (CNTFET)s,[45,46] but they are focused on phased-array design instead of the RF switch and its complete characterization. Moreover, switch operation has been shown for 5 GHz, and due to the inherent limitations of fully printed transistors speeds, it is expected that the switch cannot operate at higher frequencies. Nonetheless, to the best of author's knowledge, no MIT-based RF switch has ever been demonstrated through a printing process. One of the possible reasons for this paucity may be the lack of availability of a suitable ink for RF-switching purposes. If an RF switch can be printed, its cost can be brought down considerably.

As mentioned above, VO_2 is a promising phase-change material suitable for RF-switching applications. This work demonstrates a novel VO_2 ink and a printing process that has enabled extremely low-cost (as low as one-cent) fully printed RF switches that can be triggered either

thermally or electrically. Two switching configurations, namely series and shunt, have been demonstrated. These switches have shown decent performance from very low frequencies up to 40 GHz. In the OFF state, isolations ranging of 30–15 dB have been achieved (from low to high frequency respectively). In the ON state, insertion loss of around 1 dB has been achieved for shunt configuration and around 3dB for the series configuration. More than a 10^2 ON/OFF ratio and a switching speed of 0.4 µs has also been achieved. Finally, a frequency-reconfigurable antenna, printed on a flexible Kapton substrate along with a printed VO_2 switch, has been demonstrated as a proof of concept.

2. Results and Discussion

2.1. Synthesis and Characterization of VO_2 Ink

After the preparation of VO_2 nanoparticles, with full details provided in the experimental section, the crystalline phase is characterized by X-ray diffraction (XRD) analysis. It is observed that as-synthesized VO_2 nanoparticles comprise a mixture of VO_2 (A) and VO_2 (M) phases, as shown in **Figure 1** (a). However, the required phase is the monoclinic VO_2 phase, which shows only the metal-insulator transition at ~68 °C. To get a pure VO_2 (M) phase, different annealing conditions, such as annealing in air and vacuum, were investigated. The sample annealed in air revealed un-resolved XRD peaks in addition to VO_2 (M) phase, as shown in supporting Figure S1. However, a pure phase was achieved after annealing the nanoparticles at 300 °C for 3 h in vacuum condition, as shown in Figure 1 (b). The XRD peaks in Figure 1 (b) can be indexed to VO_2 (M) phase, which is well matched to JCPDS No. 72-0514.[48] The reversible phase transition of the VO_2 nanoparticles was further confirmed by differential scanning calorimetry (DSC), as shown in Figure 1 (c). The exothermic peak indicates an MIT temperature at ~70 °C during heating, and ~50 °C during the cooling cycle. The DSC analysis

confirms the first-order phase transition from monoclinic to tetragonal with temperature. Figure 1 (d) shows the morphology of annealed VO_2 nanoparticles which are primarily spherical and aggregated with average particle size smaller than 100 nm. For the ink-formulation, annealed VO_2 nanoparticles were treated with oleic acid to make them compatible with organic solvents, and were then dispersed in the mixture of 3.5 ml 2-methoxy ethanol, 0.3 ml chlorobenzene and 0.2 ml ethanol. The resulting ink solution, as shown in the inset of Figure 1 (d), was then stirred for 24 h. Subsequently, the formulated ink was filtered by 0.45 µm polypropylene (PP) Whatman paper before jetting.

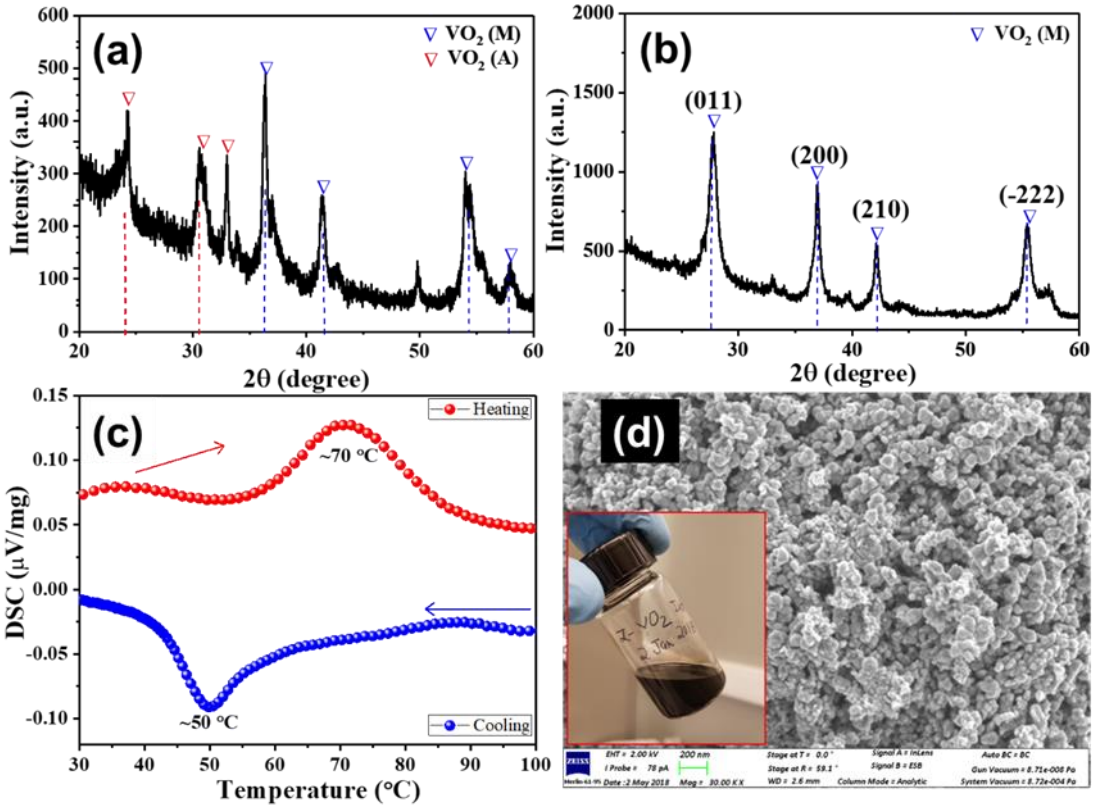

Figure 1. The XRD spectra of (a) as-prepared VO_2 nanoparticles, (b) after annealing at 300 °C for 3 h in vacuum, (c) DSC analysis and (d) SEM image of annealed VO_2 nanoparticles. The inset in (d) is showing the camera image of as-formulated VO_2 ink.

2.2. RF Switch Configurations

The RF switch design is based on a coplanar waveguide (CPW) transmission line, as shown in Figure 2 (c). The CPW line has a center conductor that carries the signal, and it is sandwiched between two ground planes. This structure can be easily tested with ground-signal-ground (GSG) probes. The layouts of two different RF switch configurations (i.e., shunt switch and series switch) are shown in Figure 2 (d) and (e), respectively. For the shunt switch, VO_2 is printed such that it covers an entire part of the CPW line that includes the signal and the ground traces. The way it operates is that, at room temperature (or zero excitation current), the VO_2 film is insulating. It thus allows the RF signal to pass through the metallic signal trace (this is termed as the ON condition for the shunt switch). When the VO_2 film is activated, through thermal or current excitation, it becomes conductive and thus shorts the signal trace to the ground traces. Nothing is transmitted through the CPW line under this state (this is termed as the OFF state of the shunt switch). In contrast to the shunt switch configuration, VO_2 film is printed in a small gap in the signal trace for the series switch configuration (Figure 2 (e)). At room temperature (or zero current excitation), VO_2 film is insulating, thus the gap in the signal line does not allow any signal transmission (this is termed as the OFF state for the series switch). When the VO_2 film is activated, through thermal or current excitation, it becomes conductive and thus bridges the gap in the signal trace, allowing signal transmission (this is termed as the ON state for the series switch).

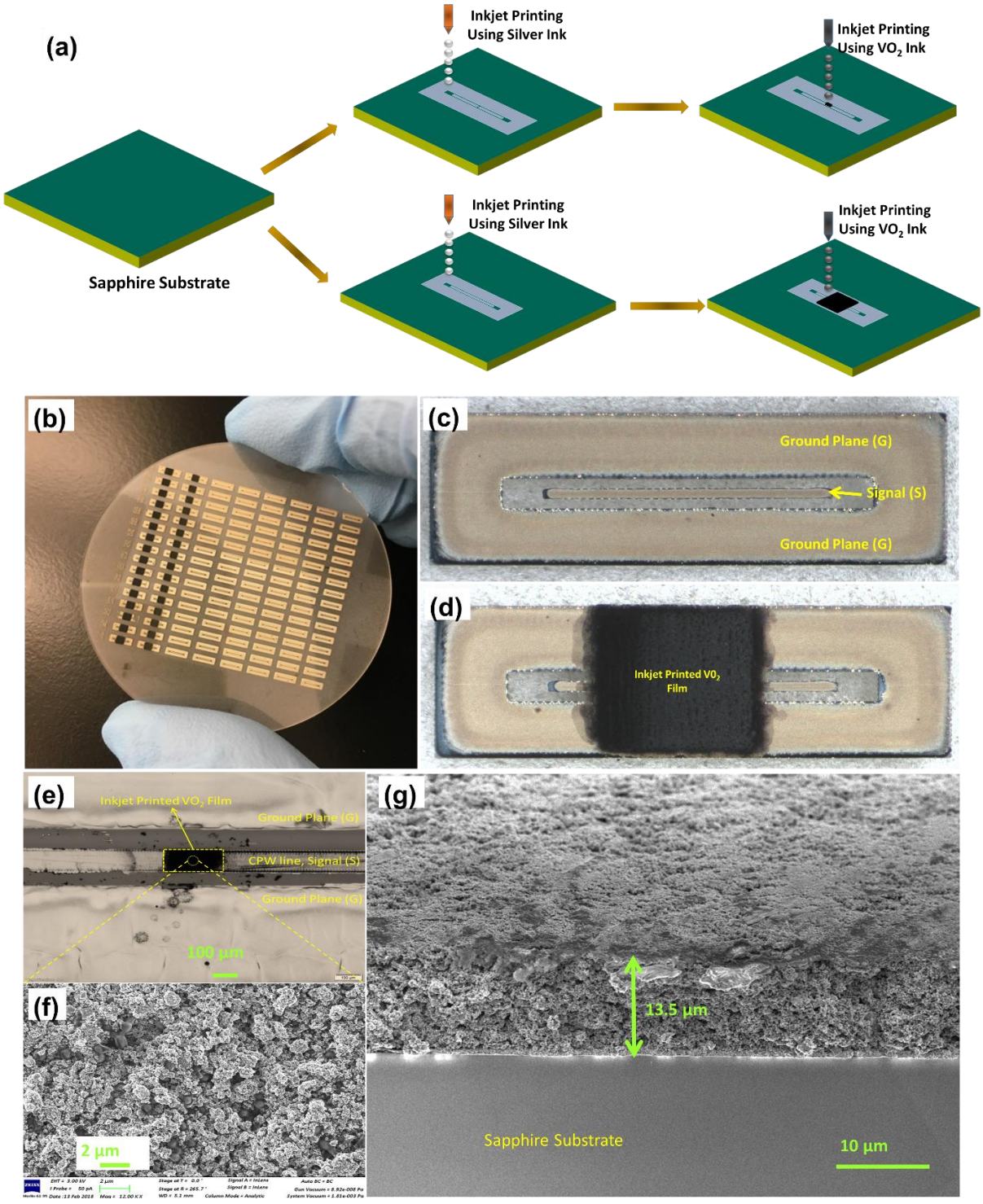

Figure 2. (a) Schematic diagram of the fabrication process for fully inkjet-printed VO_2-based RF switch with series (upper branch) and shunt switch (lower branch). (b) Photo image of fabricated series and shunt switches on Sapphire wafer. Microscopic images of (c) Inkjet-printed CPW structure for shunt switches and (d) Inkjet-printed VO_2 film on top of printed CPW structure. (e) Microscopic image of inkjet-printed VO_2 film on top of the signal trace gap. (f) Zoomed-in SEM surface image of printed VO_2 film. (g) SEM cross-section view of printed VO_2 film.

2.3. Fabrication of Fully Inkjet-Printed RF Switch

In order to evaluate the functional properties of the VO_2 ink, fully inkjet-printed switches with series and shunt configuration were fabricated, as shown in Figure 2 (a). The upper process flow represents the fabrication of a VO_2 series switch, whereas the lower process flow is for a shunt switch. The printing process for both the switches is same, except for one step, which will be discussed later in this section. The printing process starts with the cleaning of the sapphire substrate with acetone and isopropanol (IPA) in a spin coater. A silver-nanoparticles-based ink (ANP) is used to print the shunt and series structures with six layers of metallic printing. The printed silver film thickness is around 1.5 µm after the curing step with a conductivity of around 2×10^7 S/m. For VO_2 printing, we have optimized the thickness of the VO_2 film with number of printed layers. In principle, less number of layers means thinner film which results in higher ON resistance. Similarly, more number of printed layers result in thicker VO_2 film with improved ON resistance but decreases the OFF resistance. The optimum number of VO_2 layers is selected based on acceptable isolation while maintaining minimum insertion loss. In our experiments, we have optimized the number of printed layers to be 50 (film thickness of 13.5 µm) for a good trade-off between isolation and insertion loss. Regarding printing time, if we use 10 nozzles in the shunt switch fabrication, the silver pattern would need 30s and the VO_2 pattern would need 7.5 min to complete all the passes. Please also be noted that printing the VO_2 pattern for series switch is much faster than for shunt switch because the size is only 85 µm by 300 µm (compared with 1 mm by 1 mm in shunt switch). The alignment between the silver layer and VO_2 layer is simply achieved by entering the printing origin offset of these two patterns in the software. The only difference between series and shunt configurations printing is that, in the case of a series structure, the signal trace is printed using another high-resolution inkjet printer called super inkjet (SIJ) printer, which is capable of printing sub-10 µm traces.[49] One hundred layers of silver ink were printed to realize a signal trace with a 20 µm gap in the center to accommodate the VO_2 switch. The VO_2 ink is printed in this gap of the CPW line with

dimensions of 85 µm by 300 µm. For the shunt switch, VO_2 ink is printed on a 1 × 1 mm area in the center, which covers the signal and ground traces, as well as the gaps between the signal and the ground.

After printing, the samples are cured in a vacuum oven at 200 °C for 1 h to evaporate the ink solvents from the VO_2 film while still restricting the VO_2 nanoparticles from becoming oxidized. Figure 2 (b) shows the fabricated shunt and series switches. The first two columns in Figure 2 (b) are shunt switches (see the prominent black VO_2 film), and the remaining are series switches. A zoomed-in view of the shunt switch before and after the printing of the VO_2 layer is shown in Figure 2 (c) and (d), respectively. As can be seen, the CPW structure is well defined using silver ink, and the printed VO_2 ink forms a thick layer that covers the gap.

A zoomed-in view on the gap area for series switch is shown in Figure 2 (e), where it can be seen that the VO_2 ink has been precisely printed in the gap and forms a bridge between the two signal traces. The scanning electron microscope (SEM) images for surface and cross-section of printed VO_2 film are shown in Figure 2 (f) and (g). The surface and cross-section images show the porosity in the film, but the VO_2 nanoparticles are well-connected with each other and form three-dimensional conductive pathways. The porosity is expected, due to ink-solvent evaporation and the low weight percentage of VO_2 nanoparticles (5 wt%) in the ink.

2.4. DC Characterization of Printed VO_2 Film

In order to evaluate the electrical characteristics of the printed VO_2 film, DC measurements have been performed with a four-point probe. The on-resistance (R_{ON}) and off-resistance (R_{OFF}) of the printed VO_2 films for shunt and series configurations have been evaluated by both electrical and thermal triggering, with the arrangement shown in the supporting information for

Figure S2. The measured resistances for series and shunt configurations with both thermal and electrical triggering are shown in Figure 3. As can be seen in Figure 3 (a), for series switches, the resistance value is reduced by two orders of magnitude (from 10 kΩ to less than 100 Ω) when the temperature increases from room temperature (22 °C) to around 90 °C. A similar response can be seen for the same switch, but with electrical triggering (Figure 3 (b)), where the resistance drops from 10 kΩ to 100 Ω, when the supplying current changes from 0 to 40 mA. As compared to the series switch, the shunt switch shows the resistance drop from 600 Ω to 3Ω (Figure 3 (c)) and 10 Ω (Figure 3 (d)), for thermal and electrical triggering, respectively. It must be noted that the effective VO_2 film dimension in shunt switch configuration is 2,000 µm × 50 µm, as compared to 85 µm × 20 µm for series configuration. Based on Pouillet's law, the resistance of the series configuration has been calculated, which is ~10 times more than that for shunt switches, provided the VO_2 film for both configurations has the same resistivity.

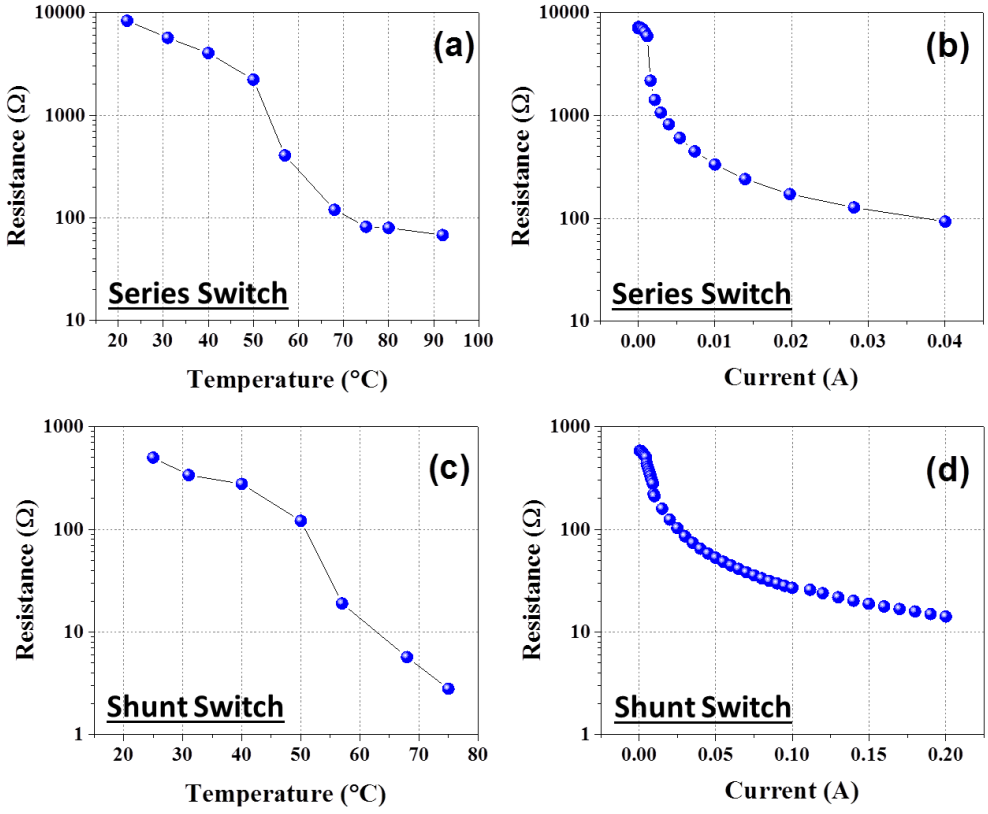

Figure 3. (a) Resistance changes for series switch at different temperature. (b) Resistance changes for series switch at different bias current. (c) Resistance changes for shunt switch at different temperature. (d) Resistance changes for shunt switch at different bias current.

It is worth mentioning here that for electrical triggering, the measurement test current has been limited to 40 mA for the series switch to avoid VO_2 film burning due to the Joule heating. This limit has been enhanced to 200 mA for the shunt switch, as it is larger in size and can thus handle more current. In addition, the ON/OFF ratio is approximately 10^2, which is consistent with both configurations and triggering mechanisms. This ON/OFF ratio is comparable to some other VO_2 switches.[16] However, some VO_2 switches have better ON/OFF ratios, such as 10^3 to 10^4.[14,15,17] The higher ON/OFF ratio for some switches is due to higher-quality VO_2 film that has been deposited by expensive nanofabrication processes, such as MOMBE, RF sputter and PLD with high vacuum and temperature conditions and ultra-pure VO_2 target. With such deposition, the VO_2 film tends to grow in a very pure, single-crystal form, which may afford a better ON/OFF ratio and a sharper transition.[18] For the proposed fully inkjet-printed VO_2 switch in this work, a certain degree of porosity is expected (true for all printed films due to the evaporation of solvents, etc.), as can be seen in Figure 2 (f) and (g). This porosity, in fact, lowers the density of the printed film as compared to the nanofabricated films and thus effects the switch performance. Apart from the porosity, environmental factors such as moisture and so on may also affect the performance, as the printing and testing of the switch have been done in the ambient environment. In future, smaller nanoparticles (~5 nm, as compared to ~50 nm in this work) and a higher loading of the nanoparticles (20% weight loading, as compared to 5% weight loading in this work) may mitigate the porosity issue. Moreover, the organic solvent used in this synthesis can be replaced with aqueous-based solvents that can reduce the carbon residuals in the film and thus improve the switch performance. Finally, better control of the environmental effects during the printing and testing stages may help in improving the switch performance. One method to do so is to add a passivation layer to protect the VO_2 particles

from the environmental effects. Having said that, even though the printing process is relatively new and immature, the RF performance of the fully printed switches presented in this work is comparable to the other non-printed VO_2-based switches, as shown in subsequent sections. It is worth mentioning here that the fully printed switch fabrication process costs a fraction of the non-printed switch fabrication processes.

2.5. RF Characterization

The RF characterization of the printed switches was performed on a probe-station with a vector network analyzer (VNA). The RF characterization is done by obtaining the scattering parameters (S-parameters) of the switch under varying stimuli (heat and current in this case). The test setup diagram is shown in supporting information Figure S3. The setup shown in Figure S3 (a) is used for thermally triggered RF measurement, whereas the one in Figure S3 (b) is used for electrically triggered RF measurement. For the thermally triggered configuration, the temperature is controlled through the thermal chuck temperature. The surface temperature of the sample is measured using a thermometer. For the electrically triggered configuration, the bias current is provided by the current source (SMU Keysight B2912A) through a bias tee.

2.5.1. Series Switch

The S-parameters for the series switch obtained through thermal and electrical triggering is shown in Figure 4 (a–d). Although full two-port S-parameters have been measured, only S_{11} and S_{21} parameters are shown here because the other two parameters, S_{22} and S_{12}, are identical to S_{11} and S_{21}, respectively. Parameter S_{11} is a measure of the reflection of the RF signal at port 1 due to impedance mismatch at that port (also known as “return loss,” when expressed in decibels). An S_{11} of 0 dB means total reflection of the applied signal at port 1, whereas an S_{11}

of −10 dB or below means good impedance matching (low or no reflection). Similarly, S_{21} is a measure of transmission of RF signal from port 1 to port 2 (also known as "insertion loss," when expressed in decibels). An S_{21} of 0 dB means 100% transmission of the signal from port 1 to port 2 without any loss. A value lower than 0 dB indicates loss of the signal from port 1 to port 2. At room temperature, the VO_2 film is insulating, so the series switch is in the OFF state. This means that no signal passes through the switch, as shown in S_{21} in Figure 4 (a). It can be seen that better than 20 dB isolation below 10 GHz, and better than 13 dB isolation up to 40 GHz has been achieved (Figure 4 (a)). This can also be observed in the S_{11} graph of Figure 4 (b), where a total reflection can be seen. When the temperature is increased to 80 °C, the VO_2 channel becomes conductive, thus the signal can pass through the switch now. The S_{21} is less than −4 dB for most frequency points (Figure 4 (a)) and the S_{11} is less than −10 dB, indicating good matching (Figure 4 (b)). For electrical triggering, 50 mA of current is chosen to operate the switch, which is a compromise between low ON resistance and the device-breakdown limit. The electrically triggered switch has an insertion loss of less than 3 dB for frequencies up to 40 GHz (Figure 4 (c)) and the return loss is around 10 dB over the measurement frequency ranges (Figure 4 (d)).

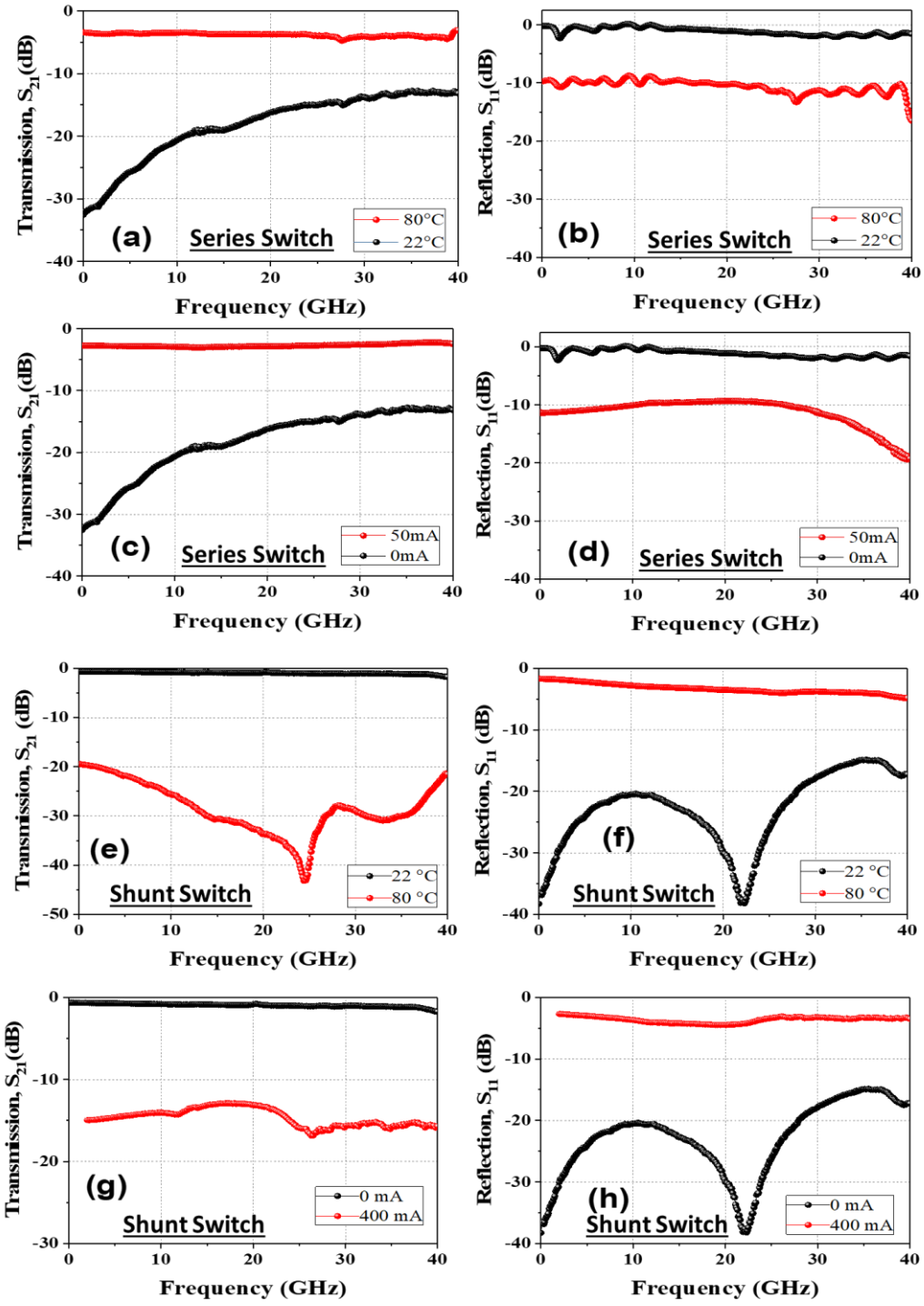

Figure 4. The RF performance of series switch and shunt switch triggered by thermal and electrical mechanism. (a) S_{21} and (b) S_{11} of series switch at room temperature and at 80 °C. (c) S_{21} and (d) S_{11} of series switch with no current bias and with 50 mA current bias. (e) S_{21} and (f) S_{11} of shunt switch at room temperature and at 80 °C. (g) S_{21} and (h) S_{11} of shunt switch with no current bias and with 400 mA current bias.

These tests confirm that both the thermally triggered and electrically triggered switches perform in a similar fashion. For both cases, the insertion loss is around 3–4 dB, and the return loss is

about 10 dB. The insertion loss seems to be on the higher side; however, that is due to the relatively large size of the switch (in micrometers, as compared to the nanometer switches in the literature). If the effect of the dimensions can be excluded from the insertion loss value (which means the comparison can be done for a standard switch size), the value of the insertion loss shown here is comparable to other published VO_2-based switches.[14,15] Having said that, for future demonstrations, a switch of smaller length can be selected to reduce this loss. Similarly, increasing the thickness and quality of the film, for example by reducing its porosity (as discussed in detail in the "DC Characterization" section), will also help reduce this loss.

2.5.2. Shunt Switch

Similar to the series switch case, RF response has been measured for the shunt switch with both thermal and electrical triggering, as shown in Figure 4 (e–h). At room-temperature (or with no current bias), the shunt switch shows less than 1.2 dB insertion loss below 38 GHz, which goes slightly higher, to 1.7 dB at 40 GHz (Figure 4 (e)). At 80 °C, the printed VO_2 film becomes conductive, so the signal path is shorted with the ground, reflecting the RF signal completely; thus, no signal is transmitted. As depicted in Figure 4 (e), the isolation is better than 20 dB up to 40 GHz. As with the series switch, the RF performance of the shunt switch is similar for both thermal and electrical triggering (Figure 4 (g) and (h)). It may be noted that the insertion loss in the case of the shunt switch is lower, as compared to its series counterpart, because the signal does not need to go through the VO_2 film in the shunt configuration.

2.5.3. Switching Speed

For many applications, one important parameter for the RF switch is its switching speed. Switching speed describes how fast a switch can change its ON to OFF status or vice versa. In

order to characterize the switching speed, the setup shown in Figure 5 (a) has been used. In this experiment, the waveform generator acts as an RF signal source, and it provides continuous sinusoidal wave to the VO_2 switch through a bias tee, which is used to isolate the RF and DC signal sources. This signal is collected by the oscilloscope at the other end of the switch, again through a bias tee. The current source shown in the figure is used to trigger the switch from the OFF to the ON state. In order to measure the switching speed, the exact time of the triggering current pulse is also monitored through the oscilloscope, as can be seen in Figure 5 (a). Figure 5 (b) shows the transient response of the series switch, where the dotted lines show the switching time. As can be seen from Figure 5 (b), the switch can be turned on within 0.4 µs, which is comparable to a non-printed VO_2-based switch.[16] Of course, the switching speed depends on the length of the switch and can be further reduced if the length is shortened, as in the case of a study from Madan[14]. This fact has also been mentioned in a work from Dumas-Bouchiat[16], where it is shown that the switching speed is proportional to the active VO_2 volume.

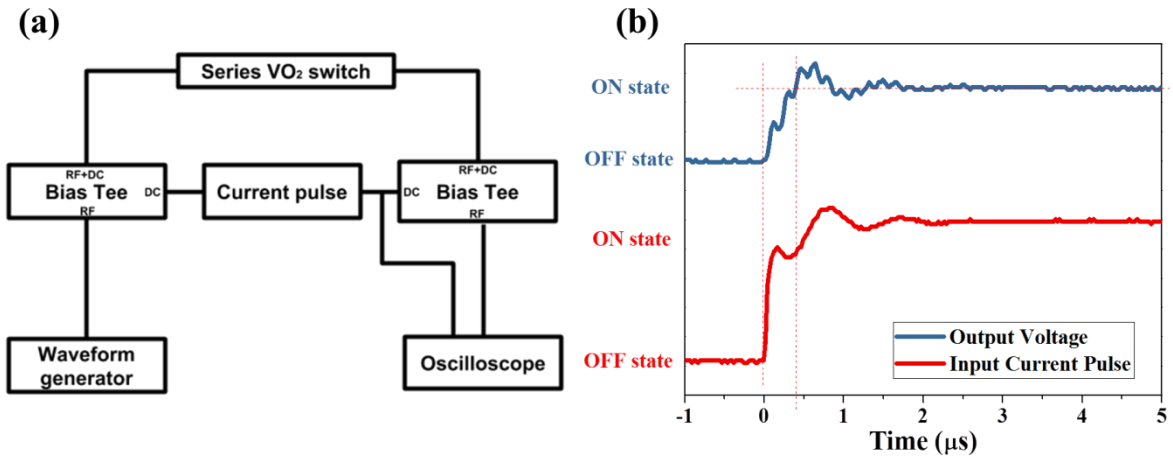

Figure 5. (a) Switching speed measurement setup and (b) measurement result for switching speed. The red curve shows that the current pulse triggers at 0 s. The blue curve shows the output voltage detected by the oscilloscope. The two vertical red dashed lines indicate the switch turn-on time.

2.6. Inkjet-Printed Reconfigurable Antenna with VO_2 Ink

As a proof of concept for VO_2-based reconfigurable RF components, a fully printed planar inverted-F antenna (PIFA) has been designed that can change its frequency of operation based on the stimulus applied. The design of the antenna is shown in Figure 6 (a). In order to make it frequency-reconfigurable, the length of the extruding arm (labeled as L5) determines the operating frequency. Since the working frequency is inversely proportional to the length of this arm (L5 = L3 + L4), for a longer arm (L5) the antenna works at a lower frequency. Similarly, a shortened arm (L3) shifts the antenna's operating frequency to a higher value.

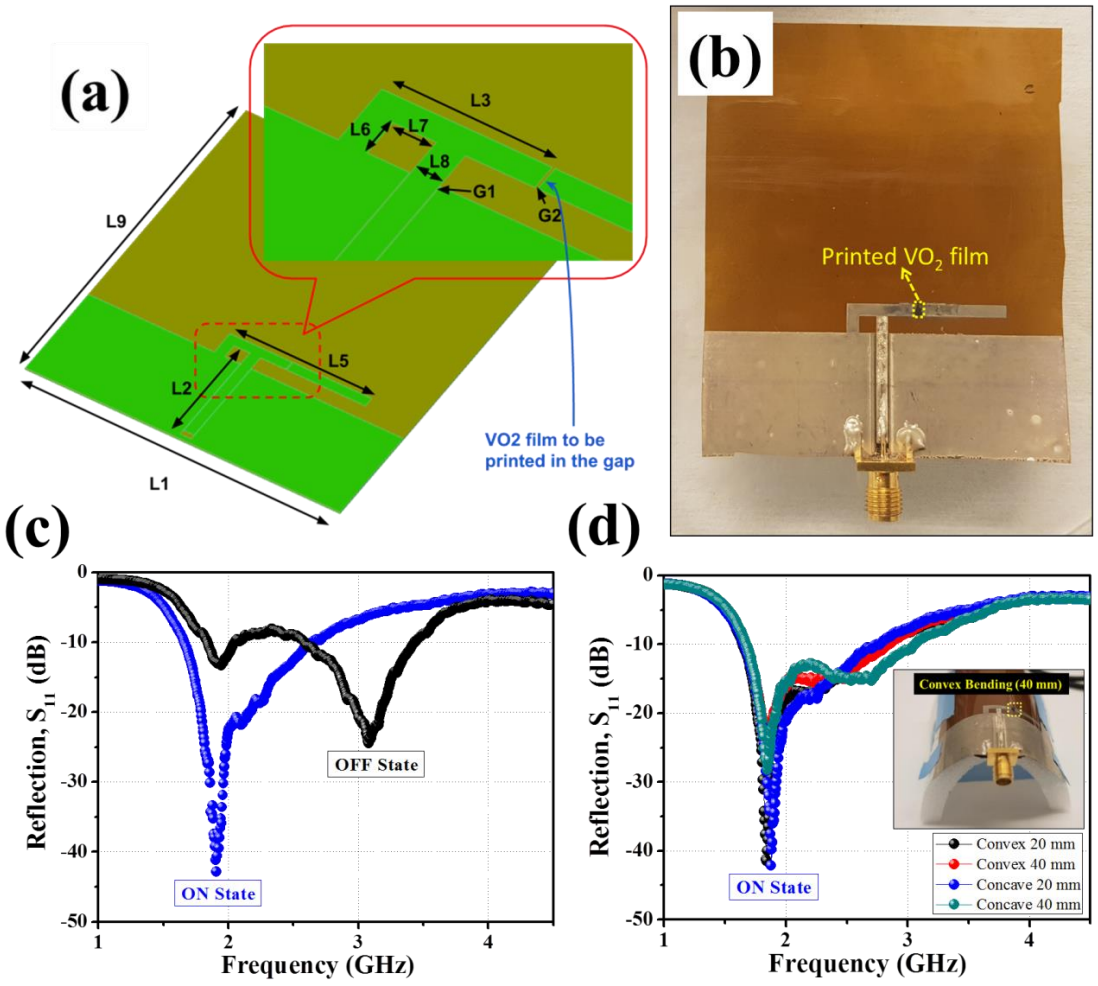

Figure 6. (a) 3D depiction of as-design PIFA antenna, (b) fabricated prototype. The measured reflection coefficient of the antenna with the VO_2 switch at (c) ON/OFF state in flat condition and (d) with different bending condition at ON state. (d) The photograph showing printed configurable antenna bending at various degrees and directions. The inset in (d) shows the photograph image of a printed configurable antenna bending 40 mm in a convex direction.

The antenna has been printed using in-house developed silver-organo-complex-based (SOC-based) ink.[31] The fabricated PIFA antenna is shown in Figure 6 (b), where VO_2 ink is printed in the gap located in the middle of antenna arm. At room temperature, the VO_2 layer exhibits insulating behavior and thus isolates the two sections (L3 and L4), with effective arm length of up to only L3. This shorter antenna works at a higher frequency (3.5 GHz). This state is termed the "OFF state" for theVO_2 switch. When the temperature is increased to 80 °C, the VO_2 film changes its phase and becomes conductive. The switch now acts as a bridge between L3 and L4 and extends the arm length, so the antenna now operates at a lower frequency (2.4 GHz). This state is termed the "ON state" for theVO_2 switch. The gap location and length of L3 and L4 in this PIFA antenna are carefully designed so that the lower frequency operates at a 2.4 GHz band and the higher frequency at 3.5 GHz. These two bands are selected because the 2.4 GHz band works for WiFi, Bluetooth and Zigbee applications, whereas the 3.5 GHz band is suitable for the upcoming 5G communication applications.

The RF performance of the PIFA antenna has been evaluated using a VNA to measure its reflection coefficient (S_{11}), as shown in Figure 6 (c) and (d). At room temperature, with the VO_2 switch in OFF state, S_{11} shows the antenna to operate within the bands of 2.57–3.4 GHz (Figure 6 (c)). The start frequency and stop frequency at −10 dB define the bandwidth. In the ON state, the antenna operates within the bands of 1.6–2.6 GHz (Figure 6 (c)). Further testing in bent conditions has been performed as well, as shown in Figure 8 (d). The antenna's consistent performance for different bend positions confirm its operation on flexible substrates.

3. Conclusions

In this work, we have shown extremely low-cost—on the order of cents—fully printed RF switches based on a novel VO_2-based ink. The paper covers the development of this ink to RF

switch design, fabrication and characterization. A frequency-reconfigurable antenna employing the printed VO_2 switch has been demonstrated, as a proof of concept. Two different types of RF switch implementations have been shown, namely, shunt and series switches. Moreover, two different switch-activation mechanisms, thermal and electrical, have also been investigated. These switches have shown good performance from very low frequencies up to 40 GHz. In the OFF state, isolations ranging from 30–15 dB have been achieved (from low to high frequency, respectively). In the ON state, insertion loss of around 1 dB has been achieved for shunt configuration and around 3 dB for the series configuration. A more than 10^2 ON/OFF ratio and a switching speed of 0.4 µs have also been achieved. The promising results of the fully printed RF switches indicate that they are very suitable for low-cost and reconfigurable RF components on flexible platforms. However, some limitations should also be noted such as the minimum feature size of 20 µm is used in this experiment, whereas a reduced feature size could potentially improve the insertion loss. In addition, the VO_2 film quality still has ample room to improve. A higher ON/OFF ratio and sharper metal-isolator transition is expected after employing high-quality VO_2 film. Lastly, the excessive passes of VO_2 printing is undesirable which can be alleviated by using higher loading of VO_2 ink. All of the above-mentioned limitations are expected to be tackled to some extent in our future studies.

4. Experimental

Chemicals: As they were received without further purification, the following chemicals were used: vanadium (IV) oxide sulfate hydrate ($VOSO_4 \cdot xH_2O$, Sigma-Aldrich, 97% anhydrous), urea (NH_2CONH_2, Fisher Scientific), hydrazine hydrate (N_2H_4, Sigma-Aldrich, reagent grade, 50–60%), oleic acid [$CH_3(CH_2)_7CH = CH(CH_2)_7COOH$, technical grade, 90%], 2-methoxyethanol ($C_3H_8O_2$, Sigma-Aldrich, anhydrous, 99.8%), chlorobenzene (C_6H_5Cl, ACS reagent, 99.5%), ethanol (absolute, VWR Chemicals).

Preparation of VO_2 Nanoparticles: Prior to ink-formulation, VO_2 nanoparticles were prepared by solution process.[50] In a typical synthesis process, 2.445 g vanadium (iv) oxide sulfate hydrate (0.1 M) was dissolved in 150 ml DI water, followed by the addition of 1.8 g urea. The resultant mixture was mixed well, and then 0.9 ml hydrazine hydrate (10% hydrazine hydrate solution in water) was added drop-wise, with stirring. The final solution was then transferred into a 200 ml PPL high-temperature polymer-liner-based hydrothermal autoclave reactor. The reaction temperature was set at 260 °C for 24 h. After the completion of the reaction, the resultant black color precipitate was washed with water and ethanol and then dried in a vacuum at 70 °C for 6 h.

Fabrication of Fully Printed Switches: The sapphire wafer was purchased from Universitywafer.com with a thickness of 430 ± 15 µm and a diameter of 50.8 mm. The orientation is C-plane (0001), with the primary flat orientation of A-plane (11-20). The surface roughness is less than 0.3 nm. Before printing, the wafer was first put into a spin coater with a spinning speed of 3000 rpm for 2 min. During the spinning, 10 mL of acetone was gently poured onto the wafer surface, following which 10 mL of IPA was slowly poured. After the spinning, the wafer surface is dry and clean, and the wafer is ready to print the pattern. This step is very critical, as it alters the surface energy of the wafer so that the silver ink would not have any issues with spreading or balling up. The silver ink DGP 40LT-15C was purchased from Advanced Nano Products Inc. Before filling the cartridge, the ink was filtered using a 1 µm polytetrafluoroethylene (PTFE) filter to remove big particles in order to avoid nozzle clogging. Dimatix DMP 2831 from Fujifilm Inc. was used as the material inkjet printer. The 10 pL cartridge DMC-11610 from Dimatix was used for silver nanoparticle ink. The jetting frequency was set at 5 kHz, and the firing voltage at 22 V. The gap between the cartridge head and the substrate was set to 0.5 mm. The cartridge temperature was set to 30 °C. During the jetting, the

platen temperature was set to 30 °C. The drop spacing of 40 µm was utilized to achieve a sharp and well-defined printed pattern. In between each layer, fast curing and drying was implemented in a convection oven set at 80 °C for 5 min. After finish printing the final layers, an intense curing was conducted in the same oven for 30 min at 150 °C. This step is important to further evaporate the solvent and densify the printed layer so that high conductivity can be achieved.

For the series switch, in order to print a ~20 µm gap on the signal trace, an SIJ printer from SIJ Technology was used, as it has ability to print sub-10-µm traces. Instead of using piezoelectric inkjet technology, as a Dimatix printer does, the SIJ printer uses the electrostatic force generated by the oscillating electric field between the substrate plate and the tip of the nozzle. The generated electrostatic force induces charging of the ink from the nozzle. The same nanoparticle ink (DGP 40LT-15C) was used in this printer. The jetting frequency was set to 50 Hz, and the jetting voltage was around 280 V, but bias voltage was set to 0 V. Sinusoidal wave was used as the jetting waveform. The printing speed is fixed at 0.5 mm/s. The distance between the nozzle tip and the substrate is about 50 µm. During the printing process, the platen temperature was kept at 40 °C to ensure the quick drying of the ink while preventing the nozzle from clogging. For all printed patterns, the line spacing is 10 µm apart in the design. The curing is needed only after printing all layers; no interlayer-curing is needed. The final curing was done by putting the sample in the oven at 150 °C for 1 h.

It is recommended that the VO_2 ink should be stored in the vial and kept continuously stirred using the stirring bar to avoid the VO_2 nanoparticles from settling. A 5 µm filter was utilized before printing to get rid of the bigger VO_2 particles. Cartridge and platen temperature were set to room temperature. Jetting frequency was reduced to 1 kHz. Drop spacing was 20 µm and no inter-layer drying is needed. Firing voltage and cartridge printing height were the same as the

ANP ink, specifically 22 V and 0.5 mm, respectively. The vacuum oven was used for VO_2 film curing.

Fabrication of Fully Printed Reconfigurable Antenna: An in-house nanoparticle-free SOC ink is used to print the antenna. This type of ink features low curing temperature with economical curing equipment (i.e., Infrared radiation (IR) lamp) while retaining very decent conductivity. The dimension of the design is as follows: L1 = 60 mm, L2 = 21 mm, L3 = 11.8 mm, L4 = 15 mm, L5 = 27 mm, L6 = 3 mm, L7 = 3 mm, L8 = 2 mm, L9 = 50 mm, G1 = 0.053 mm, G2 = 0.2 mm. In total, eight layers of SOC ink was printed on the flexible Kapton substrate. After the silver pattern is cured, 200 µm × 2000 µm square of VO_2 is printed on the gap area followed by a 1-h curing at 200 °C in the vacuum. A subminiature version A (SMA) connector was mounted afterward at the edge of the antenna using conductive epoxy, which solidifies at a lower temperature in the oven.

Characterization: The electron microscope images of the surface and the cross-section of the samples were taken using a Zeiss Merlin Gemini Field Emission SEM. In lens mode and analytical mode were used during imaging to secure clear images. The thickness of the printed VO_2 and silver layers were examined using a surface profilometer from Veeco Dektak 150. A Summit semi-automated shielded probing station from Cascade Microtech Inc. was utilized to probe the sample and conduct the DC and RF measurement. A B2912A precision source and measurement unit from Keysight Technologies was used for DC 4-wire Kelvin resistance measurement. For RF measurement, RF probe I-40-A and impedance standard substrate (ISS) 101-190 from Cascade Microtech Inc. were used and calibrated before device measurement using Wincal XE 4.5 software. The VNA from Keysight Technologies was used for the RF measurement. For electrically triggered VO_2 switch evaluation, bias tee K252 from Anritsu was utilized. Furthermore, the B2912A from Keysight Technologies was used as the current source.

In the switching-speed assessment setup, the current pulse was also stimulated from B2912A, and the bias tee is the same K252 from Anritsu. The continuous sinusoidal waveform was generated by the 33622A waveform generator from Keysight Technologies. The oscilloscope DSOX2002A from Keysight Technologies was used to monitor the input trigger and output waveform.

Supporting Information
Supporting Information is available from the Wiley Online Library or from the author.

Acknowledgements

The authors Shuai Yang and Dr. Mohammad Vaseem contributed equally to this work. We acknowledge financial support from the King Abdullah University of Science and Technology (KAUST) Office of Sponsored Research (OSR).

Received: ((will be filled in by the editorial staff))
Revised: ((will be filled in by the editorial staff))
Published online: ((will be filled in by the editorial staff))

References

[1] Z. Xu, Z. Xinbo, T. C. Wah, L. K. May, *Phys. Status Solidi A* **2017**, *214*, 1600817.

[2] U. Gaurav, T. V. Shanker, *Microw. Opt. Technol. Lett.* **2017**, *59*, 1454.

[3] D. Sukomal, K. S. K, *Microw. Opt. Technol. Lett.* **2016**, *58*, 1154.

[4] Song Yong- Ha, Ahn Sang- Joon Kenny, Kim Min- Wu, Lee Jeong- Oen, Hwang Chi- Sun, Pi Jae- Eun, Ko Seung- Deok, Choi Kwang- Wook, Park Sang- Hee Ko, Yoon Jun- Bo, *Small* **2015**, *11*, 1357.

[5] F. Thome, O. Ambacher, *IEEE Trans. Microw. Theory Tech.* **2018**, *66*, 1998.

[6] Z. Imane, H. Khelifa, Y. M. C. E, *Microw. Opt. Technol. Lett.* **2018**, *60*, 462.

[7] A. Nafe, F. A. Ghaffar, M. F. Farooqui, A. Shamim, *IEEE Trans. Antennas Propag.* **2017**, *65*, 196.

[8] V. Mohammad, G. F. Abdul, F. M. Fahad, S. Atif, *Adv. Mater. Technol.* **2018**, *3*, 1700242.

[9] "SKY13408-465LF Skyworks Solutions Inc. | RF/IF and RFID | DigiKey," can be found under https://www.digikey.com/product-detail/en/skyworks-solutions-inc/SKY13408-465LF/863-1650-1-ND/5395961, **n.d.**

[10] "HMC1084LC4 Analog Devices Inc. | RF/IF and RFID | DigiKey," can be found under https://www.digikey.com/product-detail/en/analog-devices-inc/HMC1084LC4/1127-1673-ND/4476105, **n.d.**

[11] F. J. Morin, *Phys. Rev. Lett.* **1959**, *3*, 34.

[12] J. Jiang, G. Chugunov, R. R. Mansour, in *2017 IEEE MTT- Int. Microw. Symp. IMS*, **2017**, pp. 278–280.

[13] P. J. Hood, J. F. DeNatale, *J. Appl. Phys.* **1991**, *70*, 376.

[14] H. Madan, H. T. Zhang, M. Jerry, D. Mukherjee, N. Alem, R. Engel-Herbert, S. Datta, in *2015 IEEE Int. Electron Devices Meet. IEDM*, **2015**, pp. 9.3.1-9.3.4.

[15] S. D. Ha, Y. Zhou, C. J. Fisher, S. Ramanathan, J. P. Treadway, *J. Appl. Phys.* **2013**, *113*, 184501.

[16] F. Dumas-Bouchiat, C. Champeaux, A. Catherinot, A. Crunteanu, P. Blondy, *Appl. Phys. Lett.* **2007**, *91*, 223505.

[17] K. Pan, W. Wang, E. Shin, K. Freeman, G. Subramanyam, *IEEE Trans. Electron Devices* **2015**, *62*, 2959.

[18] M. Stotz, S. D. Fritze, H. Downar, J. Wenger, in *1999 29th Eur. Microw. Conf.*, **1999**, pp. 415–418.

[19] M. Giorgio, L. Alberto, W. Marion, B. Massimo, N. Vincent, P. Benoît, *Adv. Mater. Technol.* **2017**, *2*, 1700063.

[20] W. Su, B. S. Cook, Y. Fang, M. M. Tentzeris, *Sci. Rep.* **2016**, *6*, 35111.

[21] Y. Fang, M. Akbari, J. G. D. Hester, L. Sydänheimo, L. Ukkonen, M. M. Tentzeris, *Sci. Rep.* **2017**, *7*, 8988.

[22] M. F. Farooqui, A. Shamim, *Sci. Rep.* **2016**, *6*, 28949.

[23] M. F. Farooqui, M. A. Karimi, K. N. Salama, A. Shamim, *Adv. Mater. Technol.* **2017**, *2*, 1700051.

[24] Q. Yiheng, A. A. U, H. M. M. R, H. Nan-Xing, D. M. Jamal, *Adv. Funct. Mater.* **2016**, *26*, 4923.

[25] T. Carey, S. Cacovich, G. Divitini, J. Ren, A. Mansouri, J. M. Kim, C. Wang, C. Ducati, R. Sordan, F. Torrisi, *Nat. Commun.* **2017**, *8*, 1202.

[26] E. Sowade, E. Ramon, K. Y. Mitra, C. Martínez-Domingo, M. Pedró, J. Pallarès, F. Loffredo, F. Villani, H. L. Gomes, L. Terés, R. R. Baumann, *Sci. Rep.* **2016**, *6*, 33490.

[27] B. Kim, M. L. Geier, M. C. Hersam, A. Dodabalapur, *Sci. Rep.* **2017**, *7*, 39627.

[28] Y.-Y. Noh, N. Zhao, M. Caironi, H. Sirringhaus, *Nat. Nanotechnol.* **2007**, *2*, 784.

[29] S. Kim, H. Sojoudi, H. Zhao, D. Mariappan, G. H. McKinley, K. K. Gleason, A. J. Hart, *Sci. Adv.* **2016**, *2*, e1601660.

[30] G. McKerricher, J. G. Perez, A. Shamim, *IEEE Trans. Electron Devices* **2015**, *62*, 1002.

[31] M. Vaseem, G. McKerricher, A. Shamim, *ACS Appl. Mater. Interfaces* **2016**, *8*, 177.

[32] G. McKerricher, M. Vaseem, A. Shamim, *Microsyst. Nanoeng.* **2017**, *3*, 16075.

[33] H. Lee, B. S. Cook, K. P. Murali, M. Raj, M. M. Tentzeris, *IEEE Microw. Wirel. Compon. Lett.* **2016**, *26*, 419.

[34] C. Alessandro, P. Samuele, B. Sergio, *Adv. Electron. Mater.* **2016**, *2*, 1500312.

[35] N. Yuki, Y. Toshikazu, K. Kensuke, K. Reiji, H. Sachio, K. Fumitaka, H. Tatsuo, *Adv. Mater.* **2015**, *27*, 6475.

[36] F. Andreas, K. Christian, N. Mohammad, W. Alex, J. Rolf, B. Werner, B. J. R, *Int. J. Appl. Ceram. Technol.* **2015**, *12*, E164.

[37] O. Sushko, M. Pigeon, R. S. Donnan, T. Kreouzis, C. G. Parini, R. Dubrovka, *IEEE Trans. Terahertz Sci. Technol.* **2017**, *7*, 184.

[38] H. F. Castro, V. Correia, E. Sowade, K. Y. Mitra, J. G. Rocha, R. R. Baumann, S. Lanceros-Méndez, *Org. Electron.* **2016**, *38*, 205.

[39] C. L. Cho, H. L. Kao, L. C. Chang, Y. H. Wu, H. C. Chiu, *IEEE Trans. Compon. Packag. Manuf. Technol.* **2016**, *6*, 622.

[40] S. Kim, Y. Kawahara, A. Georgiadis, A. Collado, M. M. Tentzeris, *IEEE Sens. J.* **2015**, *15*, 3135.

[41] Y. Feng, L. Xie, Q. Chen, L. R. Zheng, *IEEE Sens. J.* **2015**, *15*, 3201.

[42] V. Sanchez-Romaguera, S. Wünscher, B. M. Turki, R. Abbel, S. Barbosa, D. J. Tate, D. Oyeka, J. C. Batchelor, E. A. Parker, U. S. Schubert, S. G. Yeates, *J. Mater. Chem. C* **2015**, *3*, 2132.

[43] M. Akbari, M. W. A. Khan, M. Hasani, T. Björninen, L. Sydänheimo, L. Ukkonen, *IEEE Antennas Wirel. Propag. Lett.* **2016**, *15*, 1569.

[44] M. M. Khan, F. A. Tahir, M. F. Farooqui, A. Shamim, H. M. Cheema, *IEEE Antennas Wirel. Propag. Lett.* **2016**, *15*, 1109.

[45] M. Y. Chen, D. Pham, H. Subbaraman, X. Lu, R. T. Chen, *IEEE Trans. Microw. Theory Tech.* **2012**, *60*, 179.

[46] J. Vaillancourt, H. Zhang, P. Vasinajindakaw, H. Xia, X. Lu, X. Han, D. C. Janzen, W.-S. Shih, C. S. Jones, M. Stroder, M. Y. Chen, H. Subbaraman, R. T. Chen, U. Berger, M. Renn, *Appl. Phys. Lett.* **2008**, *93*, 243301.

[47] M. A. Monne, X. Lan, C. Zhang, M. Y. Chen, *Int. J. Antennas Propag.* **2018**, DOI 10.1155/2018/4517848.

[48] L. Zhao, L. Miao, C. Liu, C. Li, T. Asaka, Y. Kang, Y. Iwamoto, S. Tanemura, H. Gu, H. Su, *Sci. Rep.* **2014**, *4*, 7000.

[49] B. Sharma, Y. Takamura, T. Shimoda, M. Biyani, *Sci. Rep.* **2016**, *6*, 26257.

[50] W. Li, S. Ji, Y. Li, A. Huang, H. Luo, P. Jin, *RSC Adv.* **2014**, *4*, 13026.

A fully printed switches have been fabricated using metal-insulator transition material based VO_2 ink, which has been completely characterized for its switching performance. These switches have shown decent performance up to 40 GHz with more than 10^2 ON/OFF ratio and switching speed of 0.4 µs. Fully printed RF switches are suitable for low-cost and reconfigurable RF components on flexible platforms.

Keywords: VO_2, RF switches, inkjet printing, MIT, additive manufacturing

S. Yang*, M. Vaseem, A. Shamim

Fully Inkjet-Printed VO_2-Based Radio-Frequency Switches for Flexible Reconfigurable Components

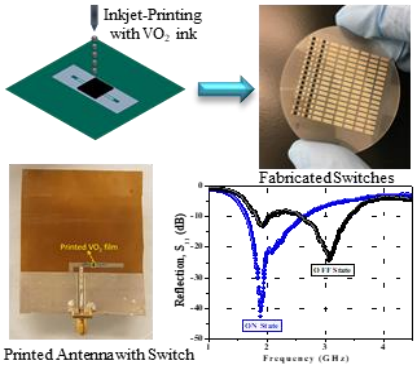

Supporting Information

Fully Inkjet-Printed VO_2-Based Radio-Frequency Switches for Flexible Reconfigurable Components

Shuai Yang, Mohammad Vaseem, and Atif Shamim*

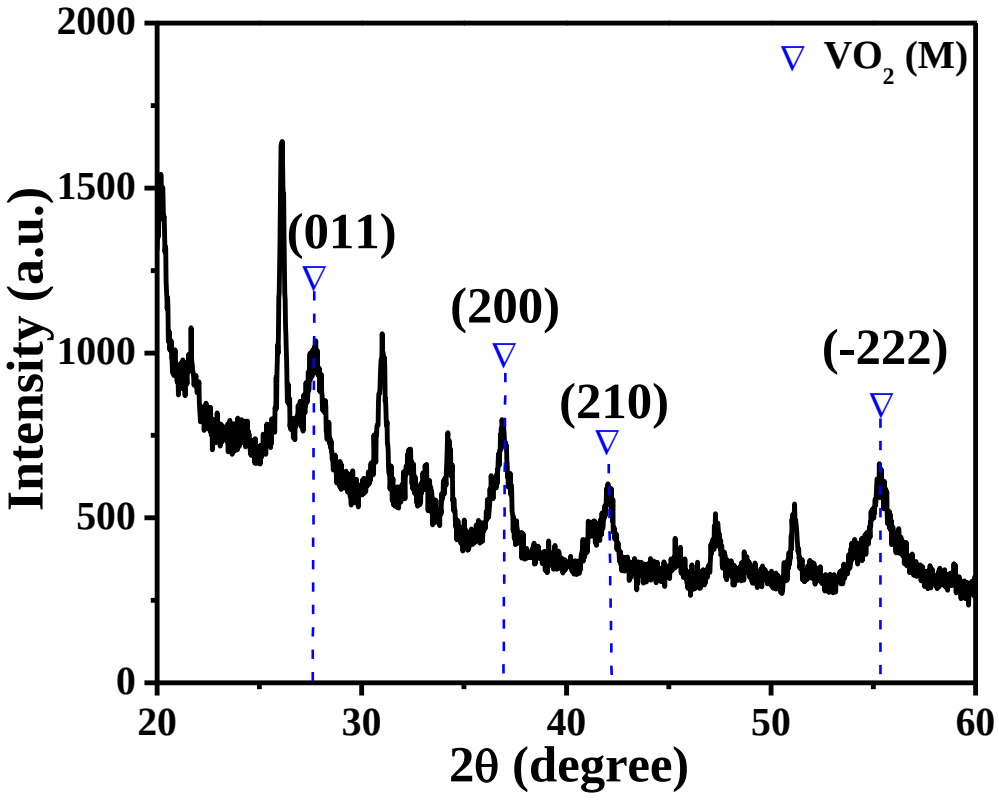

Figure S1. The XRD spectra of VO_2 nanoparticles after annealing at 300 °C for 3 h in air atmosphere

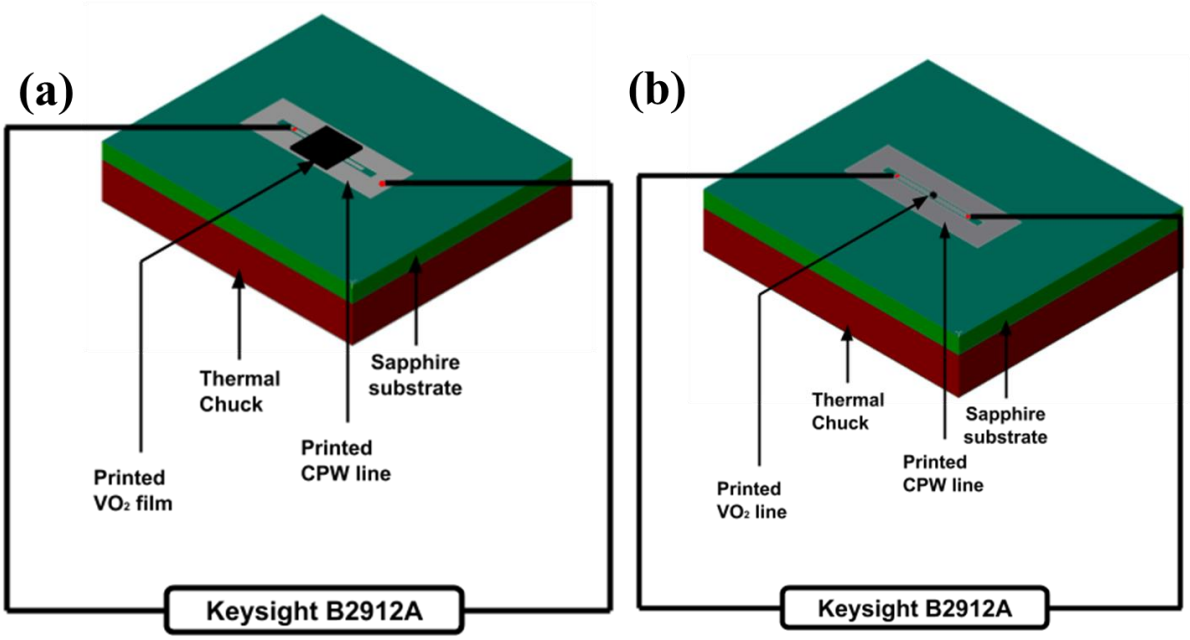

Figure S2. (a) The shunt switch setup for DC measurement. One probe is landed on one of the signal trace, while the other one is landed on the ground. The two probes are connected to a source-measurement unit (Keysight B2912A), which is used to measure the resistance. (b) The series switch setup for DC measurement. The probes are landed on the edge of each signal path. Both setups use four-wire measurement to acquire accurate resistance value.

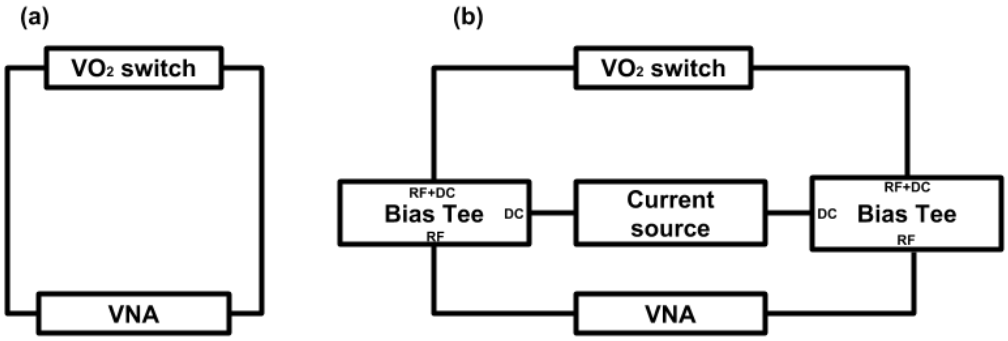

Figure S3. (a) the setup for RF measurement triggered by heat. (b) the setup for RF measurement triggered by current.